

# Noiseless Direct Quantum Communications in the Face of Noisy Entanglement

Daryus Chandra, Angela Sara Cacciapuoti, *Senior Member, IEEE*,  
Marcello Caleffi, *Senior Member, IEEE*, Lajos Hanzo, *Fellow, IEEE*

## Abstract

The availability of pre-shared entanglement among remote quantum nodes is required for facilitating quantum communications within the Quantum Internet. However, the generation and the distribution of the entanglement is inherently contaminated by quantum decoherence. Conventionally, the quantum decoherence in quantum communications is mitigated by performing the consecutive steps of quantum entanglement distillation followed by quantum teleportation. However, this conventional approach imposes a long delay. To circumvent this impediment, we propose a noiseless quantum communication scheme in the face of realistic noisy pre-shared entanglement, which eliminates the sequential steps imposing delay in the standard approach. More precisely, our proposed scheme can be viewed as a direct quantum communication scheme capable of flawless operation in the face of realistic noisy pre-shared entanglement. Our performance analysis shows that the proposed scheme offers improved qubit error ratio, yield, and goodput over the existing state-of-the-art quantum entanglement distillation based schemes, despite requiring fewer quantum gates.

## Index Terms

Quantum communication, quantum error-correction codes, quantum entanglement

## I. INTRODUCTION

Enabling quantum communications among quantum devices within the Quantum Internet [1]–[3] will ultimately lead to various groundbreaking applications. These radically new applications do not necessarily have classical counterparts [4] and they are not limited to the already well-known secure classical communications, blind computation, distributed quantum computing, and quantum secret sharing [2], [5]–[8]. Naturally, the reliable transfer of quantum information is sought across the quantum network relying on quantum channels [9], [10]. However, the quantum channels inevitably impose deleterious quantum decoherence, which inflict quantum errors [11], [12]. In the classical domain, the errors imposed by

D. Chandra, A.S. Cacciapuoti and M. Caleffi are with DIETI, University of Naples Federico II, Naples, 80125, Italy.  
L. Hanzo is with School of ECS, University of Southampton, Southampton, SO17 1BJ, UK.

the communication channels can be mitigated using error-control codes [13]. The key idea of error-control codes is to attach appropriately designed redundancy to the information bits by an encoding process, which is utilized by the decoder to correct a certain number of errors. However, observing and/or copying quantum information is not allowed in the quantum domain due to the no-cloning theorem and the quantum measurement postulate. This motivates the carefully constructed design of quantum error-correction codes (QECCs) [14]–[17].

QECCs constitute potent error mitigation techniques required for tackling the deleterious effect of quantum decoherence. Similar to the classical error-correction codes, QECCs rely on attaching redundant qubits to the logical qubits to provide additional information that can be exploited for quantum error-correction during the decoding step [18]. Interestingly, the whole encoding and decoding process can be completed without actually observing the physical qubits and thus, preserving the integrity of the quantum information conveyed by the physical qubits. In the quantum domain, the redundant qubits can be in form of auxiliary qubits initialized to the  $|0\rangle$  or  $|+\rangle$  states, or in the form of pre-shared maximally-entangled quantum states, which are assumed to be noise-free. For a two-qubit system, the maximally-entangled quantum states are represented by the Einstein-Podolsky-Rosen (EPR) pairs. The state-of-the-art studies typically assume that the EPR pairs are pre-shared among quantum devices within the quantum networks before any quantum communication protocol is initiated. Hence, the EPR pairs can be considered as the primary resource within the Quantum Internet [10].

Having pre-shared entanglement offers several beneficial features for QECCs. Firstly, it can be used for conveniently transforming some powerful classical error-correction codes that do not satisfy the symplectic criterion<sup>1</sup> into their quantum counterparts [19]–[21]. Secondly, they can also be used for increasing the error-correction capability of quantum stabilizer codes (QSCs) [22]. Indeed, there are several types of QECCs in the literature that exploit pre-shared entanglement, such as entanglement-assisted QSCs [23], entanglement-aided canonical codes [24], as well as teleportation-based QECCs [25]. However, in all the above-mentioned schemes, the pre-shared entanglement is considered to be noise-free.

In a scenario having realistic noisy pre-shared entanglement, QECCs are invoked for quantum entanglement distillation (QED) [17], [26]–[29], which is followed by quantum teleportation [30] for transferring the quantum information. QED can be viewed as a specific application of QECCs, where several copies of noisy pre-shared EPR pairs are discarded to

<sup>1</sup>A pair of classical error-correction codes having parity-check matrices  $H_x$  and  $H_z$  can be transformed to a quantum error-correction code if they satisfy  $H_x H_z^T + H_z H_x^T = 0 \pmod{2}$ .

obtain fewer but less noisy EPR pairs. In this approach, QED and quantum teleportation have to be performed subsequently, which typically imposes excessive practical delay. Additionally, state-of-the-art QED schemes will always have some residual quantum noise, unless infinitely many noisy pre-shared EPR pairs are discarded during QED. Unfortunately, this residual quantum noise is carried over to the logical qubits during the quantum teleportation process and hence it affects the integrity of the quantum information.

Having said that, in this treatise, we propose a novel solution for achieving noiseless quantum communication, despite using noisy pre-shared entanglement. Firstly, we eliminate the idealized simplifying assumption of having noise-free pre-shared EPR pairs. Secondly, we devise a scheme for avoiding the undesired delay imposed by the consecutive steps of QED and quantum teleportation. More explicitly, our proposed scheme can be viewed as a direct quantum communication scheme, which exploits the quantum noise experienced by the pre-shared EPR pairs for improving the reliability of quantum communications. As it will become more evident later in this treatise, our proposal may be deemed philosophically reminiscent of training-based equalization techniques in classical communications, which rely on pilot sequences for estimating the channel and then eliminating its impairments. Table I boldly and explicitly contrasts our proposed scheme to the existing techniques of amalgamating pre-shared entanglement and QECCs. In Table I, we explicitly indicate that our proposal relies on realistic noisy pre-shared entanglement. Naturally, our proposal is also suitable for the scenario of noise-free pre-shared entanglement, similarly to the EA-QECC schemes. In Section VI, we formally show that our proposed scheme outperforms the state-of-the-art. Our novel contributions can be summarized as follows:

- 1) We propose a new scheme for achieving noiseless quantum communications despite relying on noisy pre-shared entanglement.
- 2) We carry out the performance analysis of the proposed scheme for both error-detection and error-correction based schemes in the face of quantum depolarizing, bit-flip and phase-flip quantum channels. The results show that the proposed scheme offers competitive performance in terms of its qubit error ratio, yield, and goodput despite requiring fewer quantum gates than the existing state-of-the-art quantum entanglement distillation schemes.

---

TABLE I: Comparison of our proposed scheme with the existing approaches.

Scheme	Noisy Entanglement	Direct Transfer
Entanglement-assisted quantum error-correction codes	No	<b>Yes</b>
Quantum entanglement distillation + Quantum teleportation	<b>Yes</b>	No
Proposed	<b>Yes</b>	<b>Yes</b>

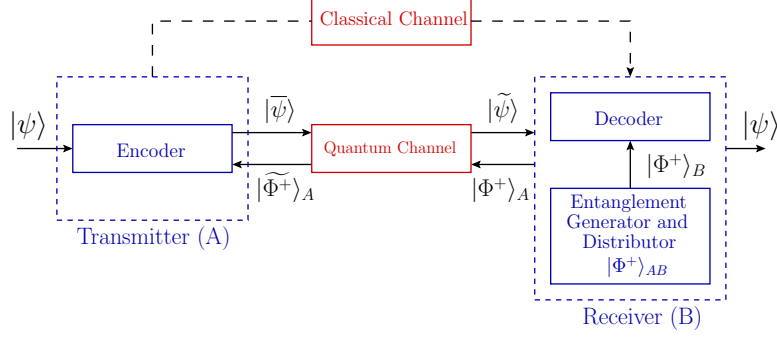


Fig. 1: The quantum communication model considered for our proposed scheme.

- 3) In case of noise-free pre-shared entanglement, the proposed scheme outperforms even the existing entanglement-assisted quantum stabilizer codes.

The rest of the treatise is organized as follows. In Section II, we commence by presenting the quantum communication model. In Section III, we detail the explicit formulation of our proposed scheme for direct noiseless quantum communication over noisy pre-shared entanglement. In Section IV, we exemplify our scheme proposed for error-detection, while in Section V, we conceive its counterpart for error-correction. In Section VI, we show the suitability of our proposal for quantum computing applications. Finally, we conclude in Section VII by also discussing some future research directions.

## II. SYSTEM MODEL

As discussed in [10], both entanglement generation and distribution are key for the Quantum Internet. The specific “location” of the device implementing these functionalities – a.k.a. the *entanglement generator and distributor* – varies among the different schemes and solutions [10]. However, there is a general agreement in the literature that the employment of the so-called “*at both end-points*” scheme is vital for the Quantum Internet by enabling on-demand communication capabilities at the quantum nodes. According to the “*at both end-points*” scheme, the entanglement generator and distributor is embedded within both the transmitter and the receiver [10]. In this light, we consider the quantum communication model depicted in Fig. 1. The model includes a transmitter (A), a receiver (B), the entanglement generator and distributor, a noisy quantum channel and a classical channel. Without loss in generality, in the figure we only highlighted the entanglement generator and distributor used at the receiver, since it is exploited by the proposed scheme. The quantum communication session commences with the generation of the EPR pairs, whose quantum state is

$$|\Phi^\pm\rangle_{AB} = \frac{1}{\sqrt{2}}(|00\rangle \pm |11\rangle)_{AB}, \quad |\Psi^\pm\rangle_{AB} = \frac{1}{\sqrt{2}}(|01\rangle \pm |10\rangle)_{AB}. \quad (1)$$

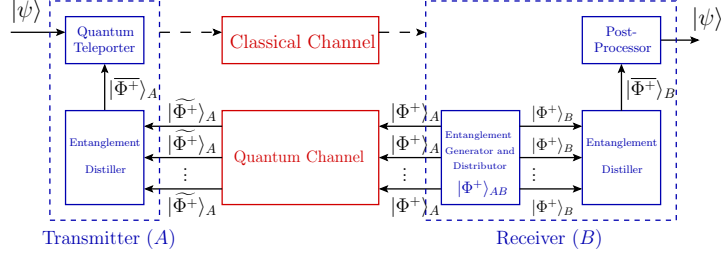


Fig. 2: The conventional quantum communication model relying on consecutive steps of quantum entanglement distillation and quantum teleportation.

In the rest of this treatise, we assume that the pre-shared EPR pairs are initialized to the quantum state of  $|\Phi^+\rangle_{AB}$ , where the subscript  $AB$  indicates that the first qubit of each EPR pair is held by  $A$  and the second qubit is held by  $B$ . In Fig. 1, the entanglement generator is located at  $B$ . Hence, the first qubit of the EPR pairs  $|\Phi^+\rangle_A$  has to be sent by  $B$  through the quantum channel, while the second qubit of the EPR pairs  $|\Phi^+\rangle_B$  is available immediately at  $B$ . After  $A$  obtains the first qubit of the EPR pairs  $|\Phi^+\rangle_A$ , it can be exploited for transmitting the quantum information embedded within the logical quantum qubit  $|\psi\rangle$ . In addition to the pre-shared EPR pairs,  $A$  and  $B$  are also connected via a classical communication channel, which is considered to be noise-free<sup>2</sup>.

The main goal of the quantum communication model of Fig. 1 is to faithfully transfer the quantum state  $|\psi\rangle$  from  $A$  to  $B$  assisted by the pre-shared EPR pairs and also by classical communications. To achieve this goal,  $A$  may exploit the noisy pre-shared EPR pairs  $|\Phi^+\rangle_A$  for appropriately encoding the logical qubits  $|\psi\rangle$  into  $|\tilde{\psi}\rangle$ , which is sent to  $B$ . In addition to the received encoded quantum state  $|\tilde{\psi}\rangle$ ,  $B$  also obtains the classical bits gleaned from the measurement of the EPR-pair members  $|\Phi^+\rangle_A$  at  $A$ . Finally,  $B$  performs a decoding procedure to reconstruct the original quantum state  $|\psi\rangle$  of the logical qubits by utilizing the qubits of the EPR-pair members  $|\Phi^+\rangle_B$  at  $B$ .

Before outlining the mathematical details of our proposal, let us briefly discuss the conventional quantum communication model that relies on the consecutive steps of QED and quantum teleportation, as portrayed in Fig. 2. Similar to the model of Fig. 1, the “*at both endpoints*” scheme is adopted. In contrast to our proposal, QED-based schemes rely on numerous copies of EPR pairs, first generated and then distributed. At the transmitter  $A$  and receiver  $B$ , the entanglement distillers discard the several copies of the noisy EPR pairs to obtain fewer but less-noisy EPR pairs. Once the QED step is completed, quantum teleportation is used for faithfully transferring the quantum state  $|\psi\rangle$  of the logical qubits from  $A$  to  $B$ . Since the

<sup>2</sup>This assumption is not restrictive since we focus our attention on the quantum noise only. In case of a realistic noisy classical channel, the well-known classical error-mitigation techniques can be implemented.

QED and the quantum teleportation are performed subsequently, the conventional quantum communication model seen in Fig. 2 imposes a longer communication delay than the model of Fig. 1. Additionally, the state-of-the-art QED schemes always have some residual quantum noise unless infinitely many noisy pre-shared EPR pairs are discarded during QED. This residual quantum noise is carried over to the logical qubits during the quantum teleportation step and it affects the integrity of the quantum information.

#### A. Error Model

In this treatise, we consider one of the most general quantum channel model, namely the quantum depolarizing channel  $\mathcal{N}(\cdot)$ , a type of quantum Pauli channel. For a single-qubit system, the quantum depolarizing channel is described by

$$\mathcal{N}(\rho) = (1 - p)\rho + \frac{p}{3}(X\rho X + Y\rho Y + Z\rho Z), \quad (2)$$

where  $\{I, X, Y, Z\}$  are the Pauli matrices and  $\rho$  denotes the density matrix of the input quantum state. The Kraus operators of  $\mathcal{N}(\cdot)$  are given by  $N_1 = \sqrt{1-p}I$ ,  $N_2 = \sqrt{\frac{p}{3}}X$ ,  $N_3 = \sqrt{\frac{p}{3}}Y$ ,  $N_4 = \sqrt{\frac{p}{3}}Z$  [11], where  $p$  is the depolarizing probability of  $\mathcal{N}(\cdot)$ .

We also consider two other types of quantum Pauli channel, i.e. the bit-flip and the phase-flip quantum channels. The other types of quantum Pauli channels are unitarily equivalent to bit-flip and phase-flip quantum channels. Hence, the ensuing analysis can be readily extended by considering suitable pre-processing and post-processing operations [31]. The quantum bit-flip channel is defined as

$$\mathcal{N}(\rho) = (1 - p_x)\rho + p_x X\rho X, \quad (3)$$

with the Kraus operators given by  $N_1 = \sqrt{1-p_x}I$  and  $N_2 = \sqrt{p_x}X$ , where  $p_x$  is the bit-flip probability. By contrast, the quantum phase-flip channel, which is characterized by the phase-flip probability  $p_z$  and by the Kraus operators  $N_1 = \sqrt{1-p_z}I$  and  $N_2 = \sqrt{p_z}Z$ , is defined as

$$\mathcal{N}(\rho) = (1 - p_z)\rho + p_z Z\rho Z. \quad (4)$$

### III. QUANTUM COMMUNICATION WITH NOISY PRE-SHARED ENTANGLEMENT

In this section, we present the general concept of our proposed scheme for performing both error-detection and error-correction. The schematic of the proposed scheme is depicted in Fig 3. Its operation commences by preparing the initialized quantum state as follows:

$$|\psi_p\rangle = |\psi\rangle^k \otimes |\Phi^+\rangle_{AB}^{n-k}, \quad (5)$$

where  $|\psi\rangle^k$  represents the quantum state of  $k$  logical qubits, while  $|\Phi^+\rangle_{AB}^{n-k}$  represents  $(n-k)$  pairs of pre-shared EPR pairs  $|\Phi^+\rangle$  between  $A$  and  $B$ . The subscripts  $A$  and  $B$  indicate that

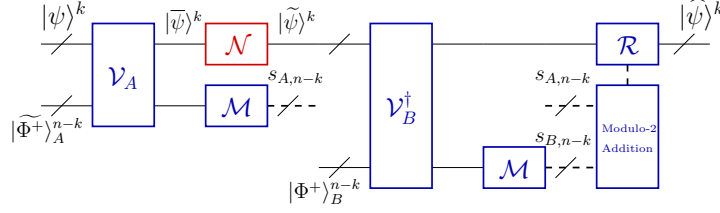


Fig. 3: The scheme proposed for performing noiseless quantum communication using noisy pre-shared EPR pairs.

half of the EPR pairs are held by  $A$  and the other half by  $B$ .

As we elucidated in Section II, the generation and the distribution of the EPR pairs to  $A$  is contaminated by the quantum noise imposed by the quantum channels. Let us denote the  $(n - k)$ -tuple Pauli operator inflicted by the quantum channel as  $P_{n-k}$ . Then, we have

$$|\widetilde{\Phi}^+\rangle_A^{n-k} = P_{n-k}|\Phi^+\rangle_A^{n-k}. \quad (6)$$

The quantum state  $|\psi\rangle^k$  of the logical qubits is encoded by a quantum encoder  $\mathcal{V}_A$ , where we exploit the noisy EPR-pair members at  $A$   $|\widetilde{\Phi}^+\rangle_A^{n-k}$ . The encoded state  $|\bar{\psi}\rangle^k$  of the logical qubits is then sent through the quantum channel  $\mathcal{N}(\cdot)$ . Let us denote the  $k$ -tuple Pauli operator inflicted by the quantum channel as  $P_k$ . Then, we have

$$|\widetilde{\psi}\rangle^k = P_k|\bar{\psi}\rangle^k. \quad (7)$$

At the receiver side, the quantum decoder  $\mathcal{V}_B^\dagger$  of Fig. 3 decodes the corrupted quantum state  $|\widetilde{\psi}\rangle^k$  with the aid of the  $(n - k)$  EPR-pair members  $|\Phi^+\rangle_B^{n-k}$  at  $B$ . To design the quantum encoder  $\mathcal{V}_A$  and the quantum decoder  $\mathcal{V}_B^\dagger$ , we impose the reversible property<sup>3</sup> on the initialized quantum state in Eq. (5), which is formulated as

$$\mathcal{V}_B^\dagger \mathcal{V}_A(|\psi\rangle^k \otimes |\Phi^+\rangle_{AB}^{n-k}) = |\psi\rangle^k \otimes |\Phi^+\rangle_{AB}^{n-k}. \quad (8)$$

**Remark.** We note that in conventional QECCs, the reversible property of a noise-free scenario can always be guaranteed, since the quantum encoder  $\mathcal{V}$  and decoder  $\mathcal{V}^\dagger$  act on the same physical qubits. By contrast, in our scheme, the quantum encoder  $\mathcal{V}_A$  only processes the logical qubits  $|\psi\rangle^k$  and the EPR-pair members at  $A$ , whilst the quantum decoder  $\mathcal{V}_B^\dagger$  only processes the logical qubits  $|\widetilde{\psi}\rangle^k$  received via the noisy quantum channel  $\mathcal{N}(\cdot)$  and the EPR-pair members at  $B$ .

By denoting the density matrix of  $|\psi_p\rangle = |\psi\rangle \otimes^k |\Phi^+\rangle_{AB}^{n-k}$  as  $\bar{\rho}$ , it is possible to reformulate

<sup>3</sup>We note that in Fig. 3 there is a little notation-abuse, since we use the symbols  $\mathcal{V}_A$  and  $\mathcal{V}_B^\dagger$  to denote the encoding and decoding performed on the qubits available at  $A$  and  $B$ , respectively. Instead, in Eq. (8),  $\mathcal{V}_A$  and  $\mathcal{V}_B^\dagger$  denote the encoder and decoder acting on the global quantum state  $|\psi\rangle^k \otimes |\Phi^+\rangle_{AB}^{n-k}$ . However, this notation abuse can be tolerated since  $\mathcal{V}_A$  and  $\mathcal{V}_B^\dagger$  in Eq. (8) leave the qubits unavailable at  $A$  and  $B$ , respectively, unchanged.

the proposed general scheme of Fig. 3 as the following supermap  $\mathcal{S}$ :

$$\mathcal{S}(\mathcal{V}_A, \mathcal{V}_B^\dagger, \mathcal{N}, \bar{\rho}) = \sum_{i,j} (V_B N_j V_A N_i) \bar{\rho} (V_B N_j V_A N_i)^\dagger. \quad (9)$$

In Eq. (9), we take into account the effects of the quantum noise inflicted by the quantum channels utilized for both the distribution of the EPR-pair members at  $A$  and for the transmission of the encoded state of the logical qubits. Furthermore, in Eq. (9),  $N_i$ ,  $N_j$  represent the Kraus operators of the quantum channels<sup>4</sup>, while  $V_A$  and  $V_B$  are the matrix representations of the quantum encoder and decoder, respectively.

The scheme proposed in Fig. 3 is completed by local measurements  $\mathcal{M}$  on the EPR pairs whose outcomes control the operator  $\mathcal{R}$  depending the particular error-control strategy implemented. Specifically, to perform the associated error-control procedure, local measurements of the EPR pairs are performed for obtaining the classical bits<sup>5</sup>  $\underline{s}_{A,n-k}$  and  $\underline{s}_{B,n-k}$ . Since no joint measurements are applied to the EPR pairs for the sake of reducing the number of quantum channels utilization, a syndrome-like quantity may be constructed from the modulo-2 addition of the classical measurement results as follows:

$$\underline{s}_{n-k} = \underline{s}_{A,n-k} \oplus \underline{s}_{B,n-k}. \quad (10)$$

It is important to note that both  $A$  and  $B$  have chosen the appropriate pre-determined measurement basis  $\mathcal{M}$  for each of the EPR pairs.

In the case of the proposed error-detection schemes, the operator  $\mathcal{R}$  of Fig. 3 acts as a discard-retain unit based on the syndrome of Eq. (10). More specifically, if the syndrome values of Eq. (10) indicate the presence of errors, i.e. the syndrome values are not zeros ( $\underline{s}_{n-k} \neq \underline{0}$ ), the operator  $\mathcal{R}$  will decide to discard the logical qubits  $|\psi\rangle^k$ , otherwise it will retain the logical qubits. By contrast, in the case of the proposed error-correction schemes, the operator  $\mathcal{R}$  represents an error-recovery procedure based on maximum-likelihood decoding relying on the syndrome values of Eq. (10). Specifically, the error-recovery procedure can be formally expressed as

$$\hat{L}_k(\underline{s}_{n-k}) = \arg \max_{L_k} P(L_k | \underline{s}_{n-k}), \quad (11)$$

where  $P(L_k | \underline{s}_{n-k})$  denotes the probability of experiencing the logical error  $L_k$  imposed on the logical qubits  $|\psi\rangle^k$ , given that we obtain the syndrome values  $\underline{s}_{n-k}$ .

<sup>4</sup>To be more precise and with a little notation-abuse,  $N_i$ ,  $N_j$  denote the extended Kraus operators of the quantum channels, which account for the specific qubits affected by the quantum channels and for the increased dimension induced by the supermap of Eq. (9), acting on the global state  $|\psi\rangle \otimes^k |\Phi^+\rangle_{AB}^{n-k}$ .

<sup>5</sup>When  $n-k$  EPR pairs are considered, the local measurements of the EPR pairs produce  $2(n-k)$  outcomes. To denote the associated vectors, we utilize the notation  $\underline{s}$ .



#### IV. ERROR-DETECTION SCHEME

In this section, we consider the error-detection of either a single logical qubit or of two logical qubits and carry out its performance analysis. We rely on Definition 1 and 2 for characterizing the performance of the proposed error-detection schemes.

**Definition 1.** The success probability  $p_s$  of the proposed error-detection schemes is defined as the conditional probability of obtaining the legitimate quantum state  $\rho$  of the logical qubits, given that we obtain the all-zero syndrome values  $\underline{s}_{n-k} = \underline{0}$ :

$$p_s = p(\rho | \underline{s}_{n-k} = \underline{0}) = \frac{p(\rho \cap \underline{s}_{n-k} = \underline{0})}{p(\underline{s}_{n-k} = \underline{0})}. \quad (12)$$

The relationship between the qubit error ratio (QBER) and the success probability  $p_s$  can simply be defined as  $\text{QBER} = 1 - p_s$ .

**Definition 2.** The yield  $Y$  of the proposed error-detection schemes is defined as the ratio of  $k$  logical qubits retained after the detection using  $(n - k)$  noisy pre-shared EPR pairs, i.e.:

$$Y = \left( \frac{k}{n - k} \right) p(\underline{s}_{n-k} = \underline{0}). \quad (13)$$

Readers from the classical communication field may notice the relationship between the *yield* and *goodput* metrics. While yield has been widely used in the QED literature, goodput is a common metric utilized for normalizing the performance of classical coded communication systems with respect to the associated coding rate. The notion of goodput in the quantum domain is clarified in [32], where it is used for comparing the performance of various QECCs exhibiting different quantum coding rates and for determining their performance discrepancies with respect to the quantum capacity also known as the quantum hashing bound. We underline that yield and goodput are not the same metric, although they are intimately linked. More specifically, the goodput  $G$  is defined as the product of the success probability of a given QECC by its quantum coding rate [32], i.e.  $G = \left( \frac{k}{n} \right) p_s = \left( \frac{k}{n} \right) (1 - \text{QBER})$ . Therefore, the goodput of our proposed scheme may be reformulated as in Definition 3.

**Definition 3.** The goodput of the proposed error-detection schemes is defined as the product of the success probability by the ratio of  $k$  logical qubits to the  $(n - k)$  noisy pre-shared EPR pairs:

$$G = \left( \frac{k}{n - k} \right) p_s = \left( \frac{k}{n - k} \right) (1 - \text{QBER}). \quad (14)$$

By comparing Def. 2 and Def. 3 we can observe the intrinsic relationship between the yield and the goodput.

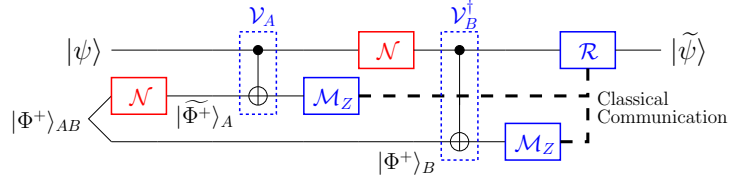


Fig. 4: The quantum circuit conceived for performing a single-qubit error-detection using a single noisy EPR pair.

#### A. Error-Detection for A Single Logical Qubit

Let us consider the proposed single qubit error-detection scheme depicted in Fig. 4, which utilizes only a single noisy EPR pair. Specifically, the encoding and decoding circuit of Fig. 3 is detailed in Fig. 4. We design the quantum encoder and decoder for ensuring that the reversible condition of Eq. (8) is satisfied. The quantum encoder  $\mathcal{V}_A$  and quantum decoder  $\mathcal{V}_B^\dagger$  of Fig. 4 can be represented using unitary matrices as follows:

$$V_A = |0\rangle\langle 0| \otimes I \otimes I + |1\rangle\langle 1| \otimes X \otimes I, \quad V_B = |0\rangle\langle 0| \otimes I \otimes I + |1\rangle\langle 1| \otimes I \otimes X. \quad (15)$$

By scrutinizing Eq. (15), it is readily seen that the reversible property is indeed satisfied, i.e.  $\mathcal{V}_B^\dagger \mathcal{V}_A (|\psi\rangle \otimes |\Phi^+\rangle_{AB}) = |\psi\rangle \otimes |\Phi^+\rangle_{AB}$ . The performance of the scheme proposed in Fig. 4 is characterized by Proposition 1.

**Proposition 1.** The success probability of the error-detection scheme depicted in Fig. 4 in the face of quantum depolarizing channels relying on a single noisy EPR pair is given by:

$$p_s = 1 - \frac{2p}{3} - \mathcal{O}(p^2), \quad (16)$$

while the yield is given by:

$$Y = 1 - \frac{4p}{3} + \frac{8p^2}{9}. \quad (17)$$

*Proof:* Please refer to Appendix A. ■

We compare our proposed scheme to the state-of-the-art QED followed by quantum teleportation schemes of Fig. 2. Specifically, we compare the scheme proposed in Fig. 4 to the single-round recurrence-based QED of [27] and to the quantum stabilizer code (QSC)-based QED of [17], [28], [29] having the stabilizer operator of  $S = ZZ$ . We assume that the quantum teleportation step is noise-free and therefore the QBER of the benchmark schemes is directly determined by the QBER of the associated QED scheme. Note that both the benchmark schemes require two noisy pre-shared EPR pairs, while our proposed scheme only needs a single noisy pre-shared EPR pair.

The QBER is portrayed in Fig. 5, where we label the performance of the scheme presented in Fig. 4 as ‘Proposed 1’. We observe that the QBER of the scheme presented in Fig. 4 matches

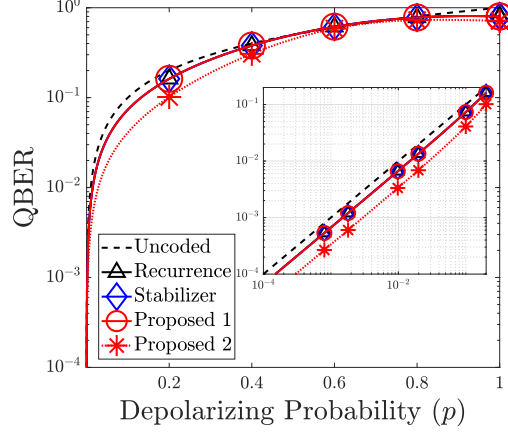


Fig. 5: The QBER of our proposed error-detection schemes compared to the existing schemes for mitigating the effect of quantum depolarizing channels. The uncoded QBER curve is given by  $\text{QBER} = p$ . The inset is the QBER in the log-log scale.

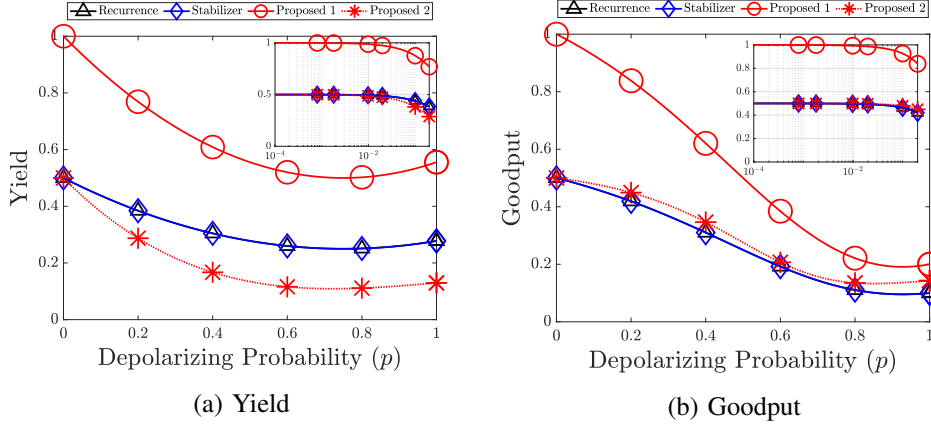


Fig. 6: The (a) yield and the (b) goodput of the proposed error-detection schemes compared to the existing schemes for mitigating the effect of quantum depolarizing channels. The insets are the yield and the goodput in the logarithmic  $x$  axis.

that of the recurrence-based and QSC-based schemes without requiring the additional quantum teleportation step, which also relies on the idealized assumption of being noise-free for both benchmarks. Furthermore, we observe that all the schemes considered are only capable of detecting a single  $X$  error. This will be confirmed later in Fig. 7(a), where we report the QBER in the presence of quantum bit-flip channels.

In Fig. 6(a), we report the performance of our proposed scheme in terms of its yield. We observe that our proposed scheme provides a significantly better yield than the benchmark schemes. Two noisy pre-shared EPR pairs are used for obtaining a single less noisy pre-shared EPR pair for both the recurrence-based and the QSC-based schemes. This means that during the process one of the noisy pre-shared EPR pairs is discarded. By contrast, our protocol

only needs a single noisy pre-shared EPR pair for achieving the same QBER performance. Finally, the goodput of our proposed error-detection scheme is presented in Fig. 6(b), which confirms again the intrinsic relationship between the yield and the goodput. Specifically, our proposal that provides a better yield, gives us also an improved goodput. Apart from its benefit of having a higher yield and goodput, our proposed scheme also offers a pair of additional advantages:

- It does not suffer from long communication delay, since it does not require the consecutive steps of performing QED followed by quantum teleportation.
- It requires fewer controlled-NOT (CNOT) quantum gates. Quantitatively, the proposed scheme of Fig. 4 requires a total of only two CNOT gates. By contrast, the recurrence-based scheme requires a total of three CNOT gates: two for a single-round recurrence and one for quantum teleportation. As for the QSC-based scheme, we need a total of seven CNOT gates: four for the measurement of stabilizer operators, two for the quantum inverse encoder, and one for quantum teleportation. The number of CNOT gates provides a reasonable estimate of how severe of the quantum error proliferation is expected to be when the realistic quantum encoder  $\mathcal{V}_A$  and the decoder  $\mathcal{V}_B^\dagger$  are error-infested as demonstrated in [33], [34]. In this case, the overall proliferation of quantum errors is heavily dependent on the number of two-qubit quantum gates. In our future work, we will carry out the performance analysis of our scheme in the presence of noisy quantum gates.

**Remark.** By invoking the simple scheme presented in Fig 4, we can attain both an improved yield and a reduced delay, despite relying on a reduced number of CNOT gates compared to the benchmarks, which is achieved without degrading the QBER.

In the following, we extend the above performance analysis of the proposed error-detection scheme to both bit-flip and phase-flip quantum channels. Specifically, in Corollary 1, we evaluate the performance in the presence of quantum bit-flip channels, while in Corollary 2, we assume the presence of quantum phase-flip channels.

**Corollary 1.** The success probability of the error-detection scheme depicted in Fig. 4 in the face of quantum bit-flip channels by relying on a single noisy EPR pair is given by:

$$p_s = 1 - p_x^2 - \mathcal{O}(p_x^3), \quad (18)$$

while the yield is formulated as

$$Y = 1 - 2p_x + 2p_x^2. \quad (19)$$

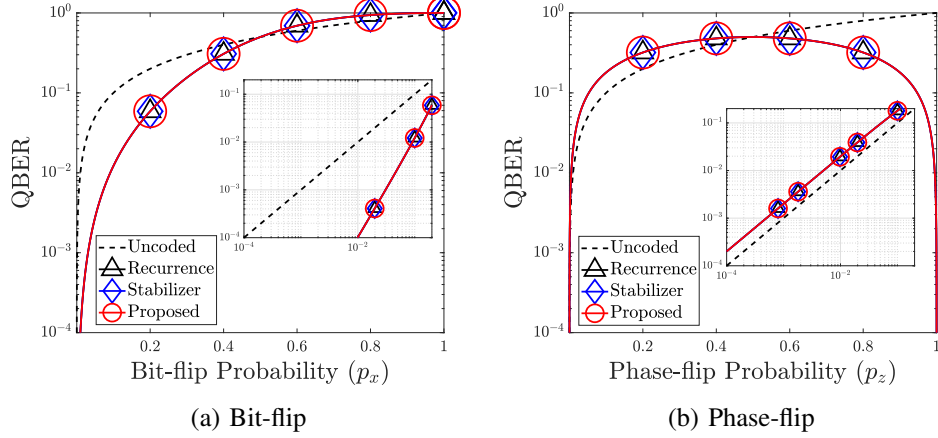


Fig. 7: The QBER of the proposed error-detection scheme compared to the existing protocols for mitigating the effect of (a) bit-flip and (b) phase-flip quantum channels. The insets are the QBER in the log-log scale.

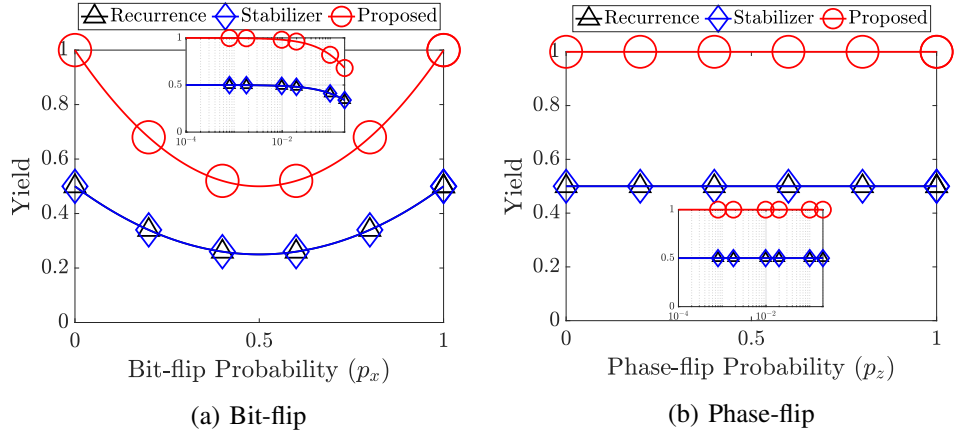


Fig. 8: The yield of the proposed error-detection scheme compared to the existing schemes for mitigating the effect of (a) bit-flip and (b) phase-flip quantum channels. The insets are the yield in the logarithmic  $x$  axis.

*Proof:* Please refer to Appendix B. ■

**Corollary 2.** The success probability of the error-detection scheme depicted in Fig. 4 in the face of quantum phase-flip channels by relying on a single noisy EPR pair is given by:

$$p_s = 1 - 2p_z + 2p_z^2, \quad (20)$$

while the yield is formulated as

$$Y = 1. \quad (21)$$

*Proof:* Please refer to Appendix C. ■

Observe from Fig. 7(a) and 7(b) that similar trends are also valid for bit-flip and phase-flip

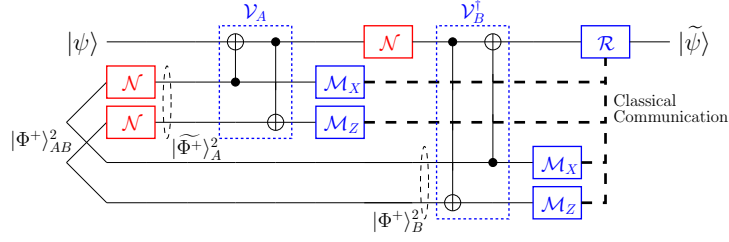


Fig. 9: The quantum circuit for performing a single-qubit error-detection using two noisy pre-shared EPR pairs.

quantum channels. Furthermore, our proposal significantly outperforms the state-of-the-art in both scenarios in terms of its yield, as depicted in Fig. 8(a) and 8(b).

In order to further generalize our analysis, let us compare the aforementioned schemes by using the same number of noisy pre-shared EPR-pairs. More specifically, we assume having two noisy pre-shared EPR-pairs for all the schemes considered. Specifically, we modify the scheme proposed in Fig. 4 as seen in Fig. 9, where the first EPR pair is measured in the  $Z$  basis ( $\mathcal{M}_Z = \{|0\rangle\langle 0|, |1\rangle\langle 1|\}$ ), while the second pair in the  $X$  basis ( $\mathcal{M}_X = \{|+\rangle\langle +|, |-\rangle\langle -|\}$ ). Let us distinguish the components of the syndrome vector in Eq. (10) according to the observation basis used for the measurement. Specifically, let us denote the syndrome component obtained when the first EPR pair is measured in the  $Z$  basis by  $s_Z = s_A \oplus s_B$  and that obtained when the second EPR pair is measured in the  $X$  basis by  $s_X = s_A \oplus s_B$ . The operator  $\mathcal{R}$  acts as follows: if  $s_Z = 0$ , the measurement of the second EPR pair is performed to obtain  $s_X$ . Otherwise, the logical qubit is discarded immediately, since there is no need to measure the syndrome value  $s_X$ , if the syndrome value  $s_Z$  already indicates that the logical qubit is corrupted. The aforementioned decision strategy is summarized as a look-up table (LUT) in Table II(a). The performance of the error-detection scheme depicted in Fig. 9 is quantified in terms of its QBER and yield presented in Proposition 2.

**Proposition 2.** The success probability of the proposed error-detection scheme of Fig. 9 operating in the face of quantum depolarizing channels by utilizing two noisy EPR pairs is:

$$p_s = 1 - \frac{p}{3} - \mathcal{O}(p^2), \quad (22)$$

TABLE II: Syndrome values and associated decision  $\mathcal{R}$  for the error-detection schemes.

(a) Scheme in Fig. 9.			(b) Scheme in Fig. 10.		
$s_Z$	$s_X$	Decision $\mathcal{R}$	$s_X$	$s_Z$	Decision $\mathcal{R}$
0	0	Retain	0	0	Retain
0	1	Discard	0	1	Discard
1	n.a.	Discard	1	0	Discard
			1	1	Discard

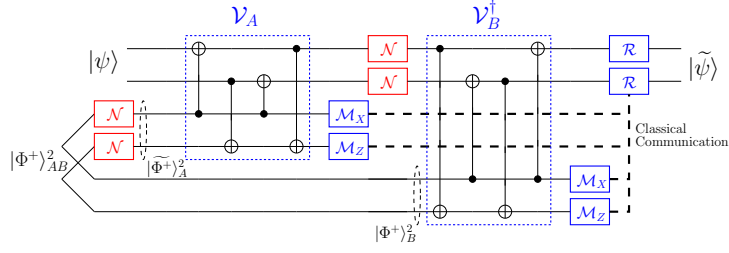


Fig. 10: The quantum circuit designed for the proposed error-detection for two logical qubits, which utilizes two noisy pre-shared EPR pairs.

while the yield is expressed as

$$Y = \frac{1}{2} \left( 1 - \frac{8p}{3} + \frac{26p^2}{9} - \frac{26p^3}{27} \right). \quad (23)$$

*Proof:* Please refer to Appendix D. ■

The QBER, yield, and goodput of the proposed scheme of Fig. 9 are portrayed in Fig. 5, 6(a), and 6(b), respectively, where it is labeled as ‘Proposed 2’. Observe in Fig. 5 that the error-detection scheme proposed in Fig. 9 outperforms all the benchmark schemes, while in Fig. 6(b), the proposed error-detection of Fig. 9 exhibits a better goodput than the benchmarks. We conclude that upon maintaining the same maximal yield, the scheme of Fig. 9 can provide better QBER. For the sake of conciseness, we refrain from reporting the performance results for the proposed scheme of Fig. 9 in the presence of bit-flip and phase-flip quantum channels.

**Remark.** By maintaining the same maximal yield and goodput as the state-of-the-art schemes, our proposed scheme provides better error-detection performance.

### B. Error-Detection for Two Logical Qubits

Let us now shift our focus to the scheme presented in Fig. 10, where we use two noisy EPR pairs for constructing an error-detection scheme for two logical qubits. Similar to the previous subsection, we commence by determining the performance of our scheme in the face of quantum depolarizing channels. Then, we evaluate the performance of the proposed scheme in mitigating the  $X$  errors imposed by quantum bit-flip channels and the  $Z$  errors inflicted by quantum phase-flip channels. As mentioned in Section II, the quantum encoder  $\mathcal{V}_A$  and decoder  $\mathcal{V}_B^\dagger$  are designed for satisfying the reversible property. The resultants quantum encoder  $\mathcal{V}_A$  and decoder  $\mathcal{V}_B^\dagger$  are seen in Fig. 10. Additionally, the decision block  $\mathcal{R}$  of Fig. 10 is represented by the LUT of Table II(b). We summarize our performance results in Proposition 3.

**Proposition 3.** The success probability of the proposed error-detection scheme of Fig. 9

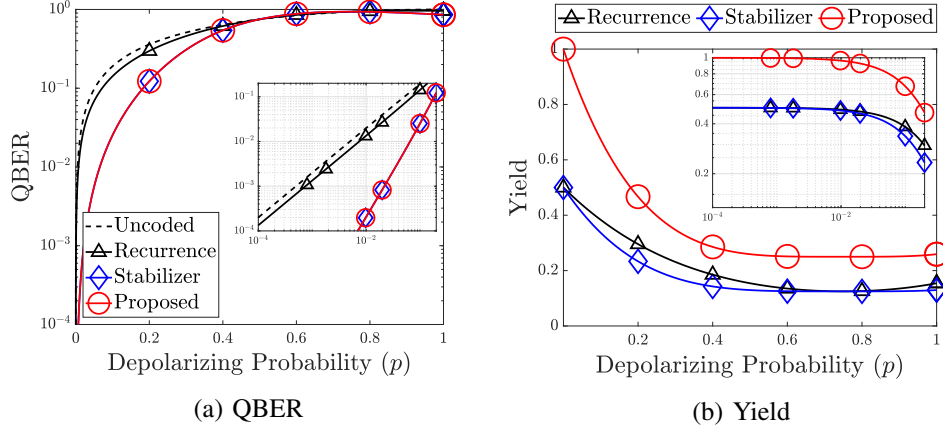


Fig. 11: The (a) QBER and the (b) yield of the proposed error-detection scheme in Fig. 10 compared to the existing schemes for mitigating the effect of quantum depolarizing channels. The uncoded QBER curve is given by  $\text{QBER} = 1 - (1 - p)^2 = 2p - p^2$ . The insets are the QBER and the yield in the logarithmic  $x$  axis.

operating in the face of quantum depolarizing channels is given by:

$$p_s = 1 - 2p^2 - \mathcal{O}(p^3), \quad (24)$$

while the yield is expressed as

$$Y = 1 - 4p + 8p^2 - \frac{64p^3}{9} + \frac{64p^4}{27}. \quad (25)$$

*Proof:* Please refer to Appendix E. ■

To benchmark the performance of the proposed scheme, we have chosen the following QED schemes. Firstly, for the recurrence-based method, we carry out two single-round distillations to obtain two less noisy EPR pairs from four noisy EPR pairs. Secondly, for the QSC-based scheme, we choose the stabilizer operators of  $S_1 = XXXX$  and  $S_2 = ZZZZ$  to apply error-detection to a set of four noisy EPR pairs. The uncoded QBER is given by  $\text{QBER} = 1 - (1 - p)^2 = 2p - p^2$ , which means that any error experienced by any logical qubit within the two qubits is considered as an error. The resultant QBER is portrayed in Fig. 11(a), while the yield is quantified in Fig. 11(b).

In Fig. 11(a), our proposed scheme can be seen to outperform the recurrence-based scheme for  $p < 0.5$ , while exhibiting an identical QBER to the QSC-based scheme. However, observe in Fig. 11(b) that our proposed scheme attains better yield than both the recurrence-based and the QSC-based schemes. Additionally, as shown in Fig. 10, the total number of CNOT gates required by the entire error-detection scheme is eight. Compared to the QSC-based scheme, which required a total of 25 CNOT gates, namely 16 CNOT gates for the stabilizer measurements, eight CNOT gates for the quantum inverse encoder, and one CNOT gate for



quantum teleportation. Hence, our proposed scheme requires significantly fewer CNOT gates while offering an identical QBER and better yield.

**Remark.** While providing an identical QBER performance to the QSC-based schemes, our error-detection scheme always provides better yield and requires fewer CNOT gates.

Next, we apply the above performance analysis of the proposed error-detection scheme to the bit-flip and phase-flip quantum channels. Specifically, in Corollary 3, we evaluate the performance of our proposal for quantum bit-flip channels, while in Corollary 4, for quantum phase-flip channels.

**Corollary 3.** The success probability of the proposed error-detection scheme of Fig. 9 operating in the face of quantum bit-flip channels is formulated as

$$p_s = 1 - 6p_x^2 - \mathcal{O}(p_x^3), \quad (26)$$

while the yield is given by

$$Y = 1 - 4p_x + 12p_x^2 - 16p_x^3 + 8p_x^4. \quad (27)$$

*Proof:* Please refer to Appendix F. ■

**Corollary 4.** The success probability  $p_s$  of the proposed error-detection scheme of Fig. 10 operating in the face of quantum phase-flip channels is expressed as

$$p_s = 1 - 6p_z^2 - \mathcal{O}(p_z^3), \quad (28)$$

while the yield is given by:

$$Y = 1 - 4p_z + 12p_z^2 - 16p_z^3 + 8p_z^4. \quad (29)$$

*Proof:* Please refer to Appendix G. ■

Observe from Fig. 12(a) that the QBER of the recurrence-based scheme is better than that of our proposed error-detection scheme as well as of the QSC-based scheme. This is due to the fact that the recurrence-based scheme is specifically tailored for detecting  $X$  errors. Hence, it mitigates more effectively the  $X$  errors imposed by the quantum bit-flip channels. By contrast, we can observe from Fig. 12(b) that the recurrence-based scheme degrades the QBER in the face of the quantum phase-flip channels, instead of improving it, since the recurrence-based scheme is not designed for detecting the  $Z$  errors. In Fig. 13(a), we portray the yield of the proposed error-detection scheme against both the recurrence-based and the QSC-based scheme for quantum bit-flip channels. Observe that our proposed scheme provides a better maximal yield. The same comment can be made for the yield obtained for quantum

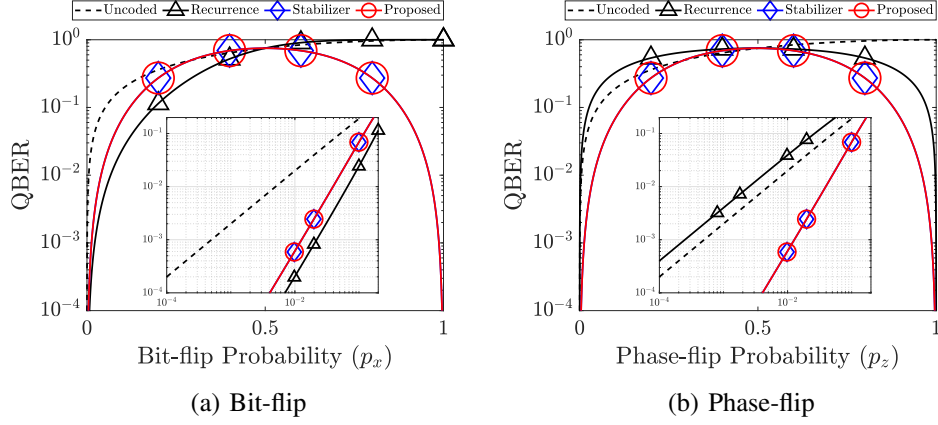


Fig. 12: The QBER of our proposed error-detection scheme of Fig. 10 compared to the existing schemes for mitigating the effect of (a) bit-flip and (b) phase-flip quantum channels. The insets are the QBER in the log-log scale.

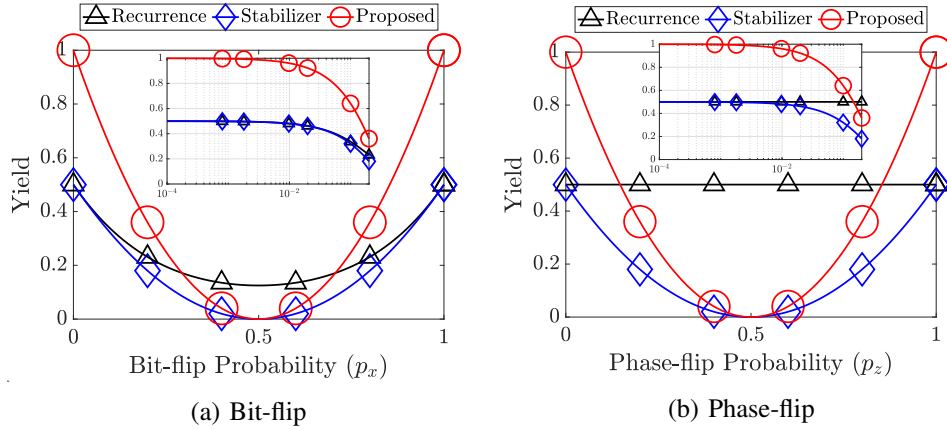


Fig. 13: The yield of our proposed error-detection scheme of Fig. 10 compared to the existing schemes for mitigating the effect of (a) bit-flip and (b) phase-flip quantum channels. The insets are the yield in the logarithmic  $x$  axis.

phase-flip channels as presented in Fig. 13(b).

## V. ERROR-CORRECTION SCHEME

Error-detection schemes provide dynamic yields, since they rely on a retain-and-discard action of the operator  $\mathcal{R}$ , while error-correction schemes provide a constant yield, since they attempt to recover the legitimate quantum state of the logical qubits from the received encoded state. Therefore, a modification of Def. 1 and 2 is required in order to accurately evaluate the performance of the proposed error-correction scheme.

**Definition 4.** The success probability  $p_s$  of the proposed error-correction scheme is defined as the sum of the conditional probabilities  $p(\hat{L}_k = L_k | \underline{s}_{n-k})$ , i.e. the sum of the probabilities that the error-recovery operator  $\mathcal{R}$  successfully applies  $\hat{L}_k = L_k$  based on the syndrome value

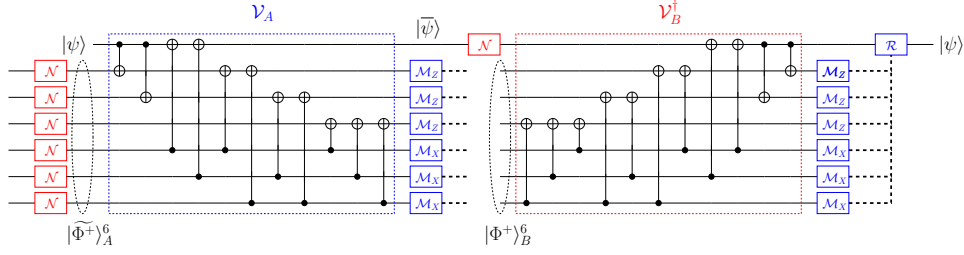


Fig. 14: The quantum encoder  $\mathcal{V}_A$  and the quantum decoder  $\mathcal{V}_B^\dagger$  for performing the proposed error-correction scheme.

$\underline{s}_{n-k}$ :

$$p_s = \sum_{L_k} p(\hat{L}_k = L_k | \underline{s}_{n-k}), \quad (30)$$

where the relationship between  $p_s$  and the QBER can be expressed as  $\text{QBER} = 1 - p_s$ .

**Definition 5.** The yield of the proposed error-correction scheme is defined as<sup>6</sup>:

$$Y = \frac{k}{n - k}, \quad (31)$$

while its goodput is similarly defined in Def. 3.

Let us now consider the quantum encoder  $\mathcal{V}_A$  and decoder  $\mathcal{V}_B^\dagger$  of Fig. 14. To investigate its error-correction performance, we have to check first that the scheme of Fig. 14 is capable of discriminating all the single-qubit error patterns based on the measured syndrome values. In Fig. 14, we can observe that the overall scheme requires six noisy pre-shared EPR pairs, which means that we have a six-bit syndrome string denoted by  $\underline{s} = s_1 s_2 s_3 s_4 s_5 s_6$ , where the indices  $i \in \{1, 2, 3, 4, 5, 6\}$  represent the EPR pair starting from the top. Therefore, for each of the single-qubit error patterns, we can evaluate the syndrome string and the associated error recovery operator, as shown in Table IV. Observe that the first three elements of the syndrome string  $\underline{s}_Z = s_1 s_2 s_3$  are exclusively used for identifying  $X$  errors, which are obtained from  $Z$  basis measurements. By contrast, the last three elements  $\underline{s}_X = s_4 s_5 s_6$  are used for identifying  $Z$  errors, which are obtained from  $X$  basis measurements. Finally, the  $Y$  errors can be identified based on the combination of  $\underline{s}_Z$  and  $\underline{s}_X$ .

First, let us investigate the performance of the proposed scheme in the face of bit-flip and phase-flip quantum channels. For quantum bit-flip channels, we have observed a total of  $2^7 = 128$  possible error patterns inflicted by the quantum bit-flip channels and calculated their

<sup>6</sup>We note that while Def. 4 is the standard definition utilized in the QECC literature, Def. 5 is not standard. Indeed, in the available QSC-based QED literature, the yield is evaluated as the quantum coding rate. In our proposal, we cannot use such a definition since the yield does not equal to quantum coding rate. Hence, we evaluate the yield as the ratio between the number of logical qubits and the number of utilized pre-shared EPR pairs.

associated syndrome strings. Based on these syndrome strings, we apply the error recovery operator  $\mathcal{R}$  given in Table IV. First, it is clear that the proposed scheme can always correct any single qubit error pattern. Additionally, the proposed scheme is also capable of correcting 28 error patterns exhibiting three  $X$  errors, seven error patterns exhibiting four  $X$  errors as well as 21 error patterns exhibiting five  $X$  errors. Therefore, the success probability of the proposed error-correction scheme of Fig. 14 in the face of quantum bit-flip channels is given by

$$p_s = 1 - 21p_x^2 + 98p_x^3 - 210p_x^4 + 252p_x^5 - 168p_x^6 + 48p_x^7. \quad (32)$$

Similarly, we can make the same observation for the proposed scheme in the face of quantum phase-flip channels. We found that the proposed scheme provides us with an identical error-correction behaviour for both bit-flip and phase-flip quantum channels. In fact, the success probability of the error-correction scheme in Fig. 14 in the face of quantum phase-flip channels is given by Eq. (32) upon substituting  $p_x$  with  $p_z$ :

$$p_s = 1 - 21p_z^2 + 98p_z^3 - 210p_z^4 + 252p_z^5 - 168p_z^6 + 48p_z^7. \quad (33)$$

Let us now extend the above calculation to the quantum depolarizing channel, where we have a total of  $4^7 = 16,384$  error patterns represented by the total number of combinations of bit-flip  $X$  errors, of phase-flip  $Z$  errors, as well as of the simultaneous bit-flip and phase-flip  $Y$  errors. Based on the observation made for quantum bit-flip channels, we know that the error-correction scheme of Fig. 14 is capable of correcting a total of  $1 + 7 + 28 + 7 + 21 = 64$  error patterns (including  $IIIIII$ ) in the face of quantum bit-flip channels. Similarly, we also have a total of 64 correctable error patterns in the presence of quantum phase-flip channels. Therefore, we observe a total of  $64 \times 64 = 4,096$  correctable error patterns in the face of quantum depolarizing channels, since we also consider the combination of  $X$  and  $Z$  errors, namely the  $Y$  errors.

After scrutinizing all 4,096 error patterns, we obtain the Pauli weight distribution of the

TABLE IV: Syndrome values and the associated error-recovery operator  $\mathcal{R}$  of the error-correction scheme presented in Fig. 14.

Error pattern $P_k, P_{n-k}$	Syndrome $\underline{s}$	Error recovery $\mathcal{R}$	Error pattern $P_k, P_{n-k}$	Syndrome $\underline{s}$	Error recovery $\mathcal{R}$
$XIIIIII$	(1 1 0 0 0 0)	$X$	$ZIIIIII$	(0 0 0 1 1 0)	$Z$
$IXIIIIII$	(1 0 0 0 0 0)	$I$	$IZIIIIII$	(0 0 0 1 0 1)	$Z$
$IIXIIIIII$	(0 1 0 0 0 0)	$I$	$IIZIIIIII$	(0 0 0 0 1 1)	$Z$
$IIIXIIII$	(0 0 1 0 0 0)	$I$	$IIIZIIII$	(0 0 0 1 1 1)	$I$
$IIIIIXII$	(0 1 1 0 0 0)	$X$	$IIIIIZII$	(0 0 0 1 0 0)	$I$
$IIIIIXI$	(1 0 1 0 0 0)	$X$	$IIIIIZI$	(0 0 0 0 1 0)	$I$
$IIIIIX$	(1 1 1 0 0 0)	$I$	$IIIIIZ$	(0 0 0 0 0 1)	$I$

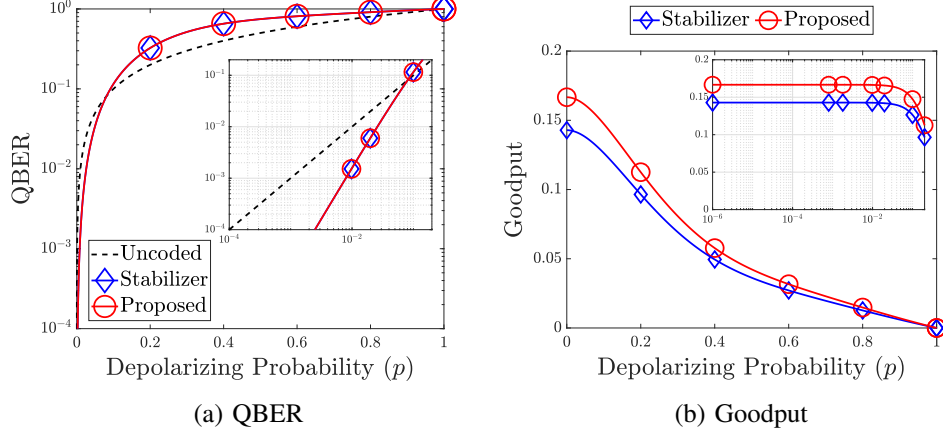


Fig. 15: The (a) QBER and the (b) goodput of our error-correction scheme proposed in Fig. 14 compared to the existing QSC-based scheme for mitigating the effect of quantum depolarizing channels. The insets are the QBER and the goodput in the logarithmic  $x$  axis.

error patterns in the face of quantum depolarizing channels as follows: one error pattern is the all-identity operator (weight = 0); 21 error patterns having weight = 1; 42 error patterns having weight = 2; 252 error patterns having weight = 3; 609 error patterns having weight = 4; 1281 having weight = 5; 1428 error patterns having weight = 6; 462 error patterns having weight = 7. This distribution is identical to that of a QSC-based scheme utilizing the stabilizer operators of the Steane code. Given that we have  $p_x = p_z = p_y = \frac{p}{3}$ , the success probability of the proposed error-correction scheme of Fig. 14 in the face of quantum depolarizing channels is given by

$$p_s = 1 - \frac{49p^2}{3} + 56p^3 - \frac{2380p^4}{27} + \frac{6160p^5}{81} - \frac{8512p^6}{243} + \frac{4824p^7}{729}. \quad (34)$$

Let us now compare the QBER of the proposed scheme to those of the QSC-based scheme. Indeed for a fair comparison, we do not consider the recurrence-based scheme, since it is an error-detection scheme, not an error-correction one. For the QSC-based scheme, we utilized the stabilizer operators of Steane code [17], [35]. The resultant QBER is depicted in Fig. 15(a), which is identical to the QBER of the QSC-based scheme utilizing the stabilizer operators of the Steane code.

Both our proposed scheme and the QSC-based scheme provide a constant level of yield, namely  $Y = \frac{1}{6}$  and  $Y = \frac{1}{7}$ , respectively, since they perform error-correction, instead of error-detection. Specifically, the proposed error-correction scheme provides better yield than the QSC-based scheme, while exhibiting the same QBER. The yield of the proposed error-correction scheme is evaluated according to Def. 5, i.e.  $Y_{\text{proposed}} = \frac{k}{n-k}$ , while the yield of the QSC-based scheme is equal to its quantum coding rate given by  $Y_{\text{stabilizer}} = \frac{k}{n}$ . Since  $n, k > 0$  and  $n > k$ , it is clear that  $Y_{\text{proposed}} > Y_{\text{stabilizer}}$ . Since both the proposed and the QSC-based

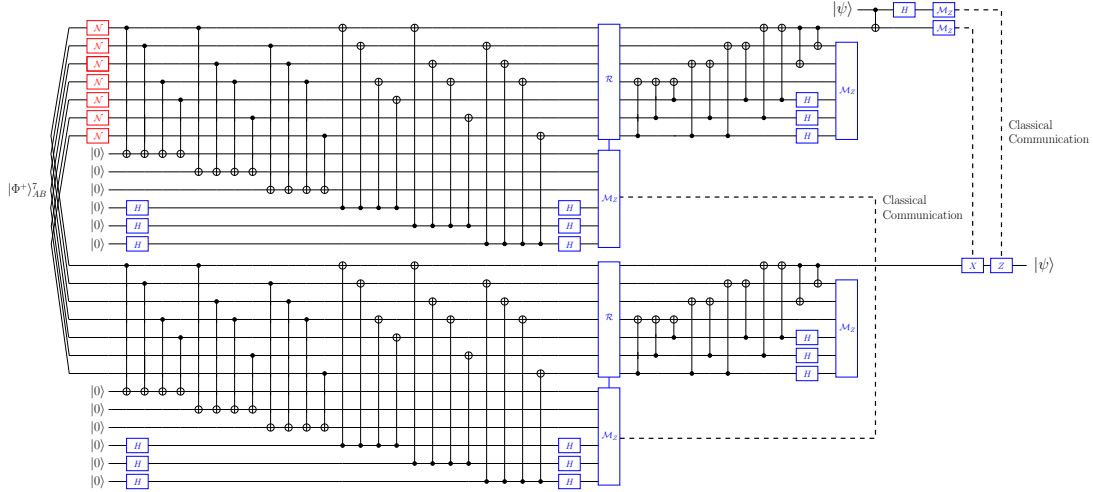


Fig. 16: The quantum circuit for performing QSC-based scheme using the stabilizer operators of Steane code followed by quantum teleportation.

schemes provide an identical QBER, while our proposed scheme offers higher yield, we can infer that the proposed scheme will also exhibit a higher goodput, as reported in Fig. 15(b). As for their complexities, our proposed scheme requires a total of 22 CNOT gates as seen in Fig. 14. By contrast, the QSC-based scheme requires a total of 71 CNOT gates, namely 48 CNOT gates for stabilizer measurements, 22 CNOT gates for the quantum inverse encoder, and one CNOT gate for quantum teleportation. To elaborate a little further on the complexity of the quantum circuit required for performing QED followed by quantum teleportation, please refer to Fig. 16, which portrays the QSC-based scheme using the stabilizer operators of the Steane code followed by quantum teleportation.

## VI. DISCUSSION: A QUANTUM COMPUTING PERSPECTIVE

In the previous sections, we have shown the advantages of our proposal in *quantum communication* applications. In this section, we demonstrate that the proposed scheme can also be adopted for *quantum computing* applications. In quantum computing applications, the quantum information is usually protected with the aid of noise-free auxiliary qubits, which may also take form of pre-shared entanglement [19]–[21], [23]–[25]. A prime example is constituted by the family of entanglement-assisted quantum stabilizer codes (EA-QSCs). Compared to the conventional QSCs, which are unassisted by noise-free pre-shared entanglement, EA-QSCs offer an error-correction capability improvement. This is reminiscent of having an additional error-free side channel between the transmitter and the receiver in the classical domain. The argument that we can always have noise-free pre-shared entanglement relies on the assumption that EPR pairs can be created abundantly and quantum entanglement distillation can be applied to them. The concept of EA-QSCs is favourable in the realms of

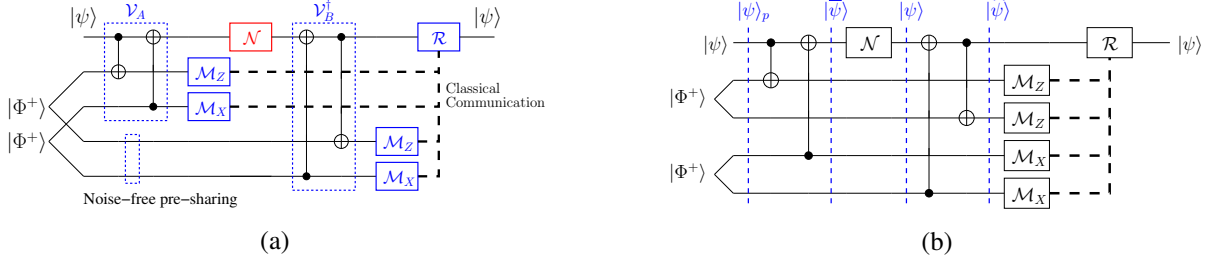


Fig. 17: (a) The quantum circuit of the proposed scheme utilizing two noise-free pre-shared EPR pairs. (b) The rearranged quantum circuit of (a) for analysis.

quantum computation, since the EA-QSCs can be readily amalgamated both with transversal implementation of quantum gates [36], [37] as well as with magic state distillation [38] for creating a universal set of fault-tolerant quantum gates. In the following, we propose an error-correction scheme that outperforms the state-of-the-art EA-QSC.

Any EA-QSC can be defined as  $\mathcal{C}[n, k, d, c]$ , where  $n$  is the number of physical qubits,  $k$  is the number of logical qubits,  $d$  is the minimum distance of the code, and  $c$  is the number of noise-free pre-shared entangled qubits. The error-detection and error-correction capability of any EA-QSC can be determined by its minimum distance  $d$ . An EA-QSC exhibiting a minimum distance  $d$  is capable of detecting  $(d - 1)$  quantum errors or correcting  $t = \lfloor (d - 1)/2 \rfloor$  quantum errors. Based on the quantum Singleton bound of EA-QSCs [23], there exists a EA-QSC capable of correcting a single-qubit error ( $d = 3$ ), which encodes one logical qubit ( $k = 1$ ) into three physical qubits ( $n = 3$ ) with the aid of two noise-free pre-shared entangled qubits ( $c = 2$ ). This specific code is denoted by  $\mathcal{C}[n, k, d, c] = \mathcal{C} = [3, 1, 3, 2]$ . In the following, we will show that by utilizing two noise-free pre-shared EPR pairs, instead of error-correction, we can achieve error elimination, implying that in this specific context, we can always obtain a noise-free logical qubit.

Let us now discuss our proposed scheme portrayed in Fig. 17(a), which is rearranged into Fig. 17(b) for facilitating our analysis. The quantum channel  $\mathcal{N}(\cdot)$  in Fig. 17(a) and 17(b) represents a quantum channel contaminating the logical qubit. According to Fig. 17(b), the quantum encoder  $\mathcal{V}_A$  is represented by the following unitary matrix:

$$\begin{aligned} V_A = & (|0\rangle\langle 0| \otimes I \otimes I \otimes I \otimes I + |1\rangle\langle 1| \otimes X \otimes I \otimes I \otimes I) \\ & (I \otimes I \otimes I \otimes |0\rangle\langle 0| \otimes I + X \otimes I \otimes I \otimes |1\rangle\langle 1| \otimes I), \end{aligned} \quad (35)$$

while the quantum decoder  $\mathcal{V}_B^\dagger$  is described by the following unitary matrix:

$$\begin{aligned} V_B = & (I \otimes I \otimes I \otimes I \otimes |0\rangle\langle 0| + X \otimes I \otimes I \otimes I \otimes |1\rangle\langle 1|) \\ & (I \otimes I \otimes I \otimes |0\rangle\langle 0| \otimes I + X \otimes I \otimes I \otimes |1\rangle\langle 1| \otimes I). \end{aligned} \quad (36)$$

It can be readily verified that the reversible property is satisfied, i.e. we have  $\mathcal{V}_B^\dagger \mathcal{V}_A (|\psi\rangle \otimes |\Phi^+\rangle_{AB}^2) = |\psi\rangle \otimes |\Phi^+\rangle_{AB}^2$ .

Upon denoting the density matrix of the initial global quantum state of  $|\psi\rangle \otimes |\Phi^+\rangle_{AB}^2$  by  $\bar{\rho}$ , the proposed scheme can be formulated with the aid of the following supermap:

$$\mathcal{S}(\mathcal{V}_A, \mathcal{N}, \mathcal{V}_B^\dagger, \bar{\rho}) = \sum_i (V_B N_i V_A) \bar{\rho} (V_B N_i V_A)^\dagger, \quad (37)$$

where  $N_i$  is the Kraus operator describing the quantum channel, while  $V_A$  and  $V_B$  represent the unitary matrices of Eq. (35) and (36). Therefore, Eq. (37) can be rewritten as:

$$\begin{aligned} \mathcal{S}(\bar{\rho}) = & (1-p)\rho \otimes |\Phi^+\rangle\langle\Phi^+| \otimes |\Phi^+\rangle\langle\Phi^+| + \frac{p}{3}(X\rho X) \otimes |\Psi^+\rangle\langle\Psi^+| \otimes |\Phi^+\rangle\langle\Phi^+| \\ & + \frac{p}{3}(Y\rho Y) \otimes |\Psi^+\rangle\langle\Psi^+| \otimes |\Phi^-\rangle\langle\Phi^-| + \frac{p}{3}(Z\rho Z) \otimes |\Phi^+\rangle\langle\Phi^+| \otimes |\Phi^-\rangle\langle\Phi^-|. \end{aligned} \quad (38)$$

After the decoding operation, we perform the measurement of the EPR pairs. Observe that we can apply  $Z$  basis measurement to the first EPR pair and  $X$  basis measurement to the second EPR pair for determining the type of Pauli error experienced by the logical qubit  $|\psi\rangle$ . To elaborate a little further, we design a scheme so that requiring a joint measurement of the EPR pairs can be avoided to reduce the complexity of the quantum encoder and decoder. We combine the classical bits of  $A$  and  $B$  of Fig. 17(b) to determine the error recovery operator  $\mathcal{R}$ .

To expound a little further, let us denote the syndrome string as  $\underline{s} = s_Z s_X$ , where  $s_Z$  is obtained from the measurement of the first EPR pair in  $Z$  basis and  $s_X$  is gleaned from the measurement of the second EPR pair in  $X$  basis. The error recovery operator associated with the syndrome value  $\underline{s} = s_Z s_X$  is portrayed in Table V. Finally, it may be inferred from Eq. (38), that after the error recovery operator  $\mathcal{R}$  of Fig. 17(a), we always obtain the legitimate quantum state  $\rho$  of the logical qubit. Hence, we have demonstrated that with the aid of two noise-free EPR pairs, instead of correcting a single-qubit achievable by an EA-QSC, we can always recover a noise-free logical qubit. Observe that when we replace the quantum channel  $\mathcal{N}(\cdot)$  by realistic noisy quantum Pauli gates, we can modify the LUT of Table V to benefit from the noise-free operation of the quantum Pauli gates.

**Remark.** This is a significant improvement compared to the existing EA-QSC  $\mathcal{C}[n, k, d, c] =$

TABLE V: Syndrome values and associated error recovery  $\mathcal{R}$  for the scheme in Fig. 17(a).

$s_Z$	$s_X$	Error recovery $\mathcal{R}$
0	0	$I$
1	0	$X$
1	1	$Y$
0	1	$Z$



$\mathcal{C}[3, 1, 3, 2]$ , which is only capable of correcting a single-qubit error by utilizing two noise-free EPR pairs. Furthermore, the 5-qubit code  $\mathcal{C}[n, k, d] = \mathcal{C}[5, 1, 3]$  of [16] is also only capable of correcting a single-qubit error. Hence, our scheme represents an improvement also with respect to [16].

## VII. CONCLUSIONS AND FUTURE RESEARCH

In this treatise, we have conceived direct noiseless quantum communication using noisy pre-shared EPR pairs. Conventionally, noiseless quantum communication tends to rely on the consecutive steps of QED followed by quantum teleportation. One of the salient benefits that we can offer is the elimination of the long communication delay imposed by the aforementioned consecutive steps, despite relying on noisy pre-shared EPR pairs. Additionally, our proposed schemes offer better QBER than the recurrence-based schemes and provide identical QBER to the QSC-based schemes. Moreover, compared to the QSC-based schemes, our proposal attains better yield, despite requiring fewer CNOT gates. We have also compared our proposed scheme to EA-QSC, which requires noise-free pre-shared EPR pairs. EA-QSCs require joint eigenvalue measurements relying on all the qubits gleaned from the EPR pairs for performing error-correction. Despite relying only on the local measurements of the EPR pairs and classical communications, we can always obtain a noise-free logical qubit. In our future research, we are interested in finding a systematic way of constructing the quantum encoder and decoder pair. In fact, we found that an arbitrary quantum encoder and decoder pair cannot always satisfy the reversible property of Eq. (8). Therefore, the sufficient and necessary conditions of generating the quantum encoder and decoder pair should be found. Furthermore, since our proposed scheme performs identically to the QSC-based schemes, it remains to be shown whether a wider range of QSCs can be directly embedded into our scheme.

## APPENDIX A: PROOF OF PROPOSITION 1

By exploiting the error model of Section II-A and by utilizing the expressions of Eq. (15), Eq. (9) can be reformulated as

$$\begin{aligned} \mathcal{S}(\bar{\rho}) = & \left[ (1-p)^2 \rho + \frac{p^2}{9} X \rho X + \frac{p^2}{9} Y \rho Y + \frac{p}{3} (1-p) Z \rho Z \right] \otimes |\Phi^+\rangle\langle\Phi^+| + \left[ \frac{p^2 \rho}{9} + \frac{p^2 X \rho X}{9} \right. \\ & \left. + \frac{p^2 Y \rho Y}{9} + \frac{p(1-p) Z \rho Z}{3} \right] \otimes |\Phi^-\rangle\langle\Phi^-| + \left[ \frac{p^2 \rho}{9} + \frac{p^2 X \rho X}{9} + \frac{p^2 Y \rho Y}{9} + \frac{p(1-p) Z \rho Z}{3} \right] \\ & \otimes |\Psi^-\rangle\langle\Psi^-| + \left[ \frac{p}{3} (1-p) \rho + \frac{p}{3} (1-p) X \rho X + \frac{p}{3} (1-p) Y \rho Y + \frac{p^2}{9} Z \rho Z \right] \otimes |\Psi^+\rangle\langle\Psi^+|, \end{aligned} \quad (39)$$

where  $\rho$  is the density matrix of the logical qubit and we assume that the quantum depolarizing channels experienced by  $|\psi\rangle$  and  $|\Phi^+\rangle_A$  exhibit an identical depolarizing probability  $p$ . After the decoding, a measurement in the  $Z$  basis of the EPR pair shared between  $A$  and  $B$  is performed. Every time we find a disagreement in the classical measurement results from the EPR pair ( $s = s_A \oplus s_B = 1$ ), the associated logical qubit is discarded, otherwise, it is retained. We note that the syndrome value of  $s = 0$  is obtained if the EPR pair is in the quantum state  $|\Phi^+\rangle$  or  $|\Phi^-\rangle$ , while the EPR pair in the state  $|\Psi^+\rangle$  or  $|\Psi^-\rangle$  gives us a syndrome value of  $s = 1$ . Hence, the probability of retaining the logical qubit is equal to the probability of obtaining the syndrome value  $s = 0$ . Based on these considerations and by accounting for Eq. (39), we can evaluate the probability of obtaining the syndrome value  $s = 0$  as  $p(s = 0) = 1 - \frac{4p}{3} + \frac{8p^2}{9}$ , which is obtained from the following error operators  $P \in \{II, IZ, XX, XY, YX, YY, ZI, ZZ\}$ . Then, based on this set of error operators, we can determine the probability of obtaining the syndrome value of  $s = 0$  and obtain the legitimate quantum state of the logical qubit  $\rho$  as  $p(\rho \cap (s = 0)) = 1 - 2p + \frac{10p^2}{9}$ , which is obtained from the following error operators  $P \in \{II, ZZ\}$ . Finally, the success probability of the scheme presented in Fig. 4 can be determined according to Def. 1 as follows:

$$p_s = p(\rho | (s = 0)) = \frac{1 - 2p + \frac{10p^2}{9}}{1 - \frac{4p}{3} + \frac{8p^2}{9}} = 1 - \frac{2p}{3} - \mathcal{O}(p^2), \quad (40)$$

which gives us an approximately linear performance improvement over the uncoded QBER as a function of  $p$ . By accounting for Def. 2, the yield is  $Y = p(s = 0)$  and the proof follows.

#### APPENDIX B: PROOF OF COROLLARY 1

The supermap of Eq. (9) of the error-detection scheme proposed in Fig. 4 operating in the face of quantum bit-flip channels is given by  $\mathcal{S}(\bar{\rho}) = [(1 - p_x)^2 \rho + p_x^2 X \rho X] \otimes |\Phi^+\rangle\langle\Phi^+| + [p_x(1 - p_x)\rho + p_x(1 - p_x)X \rho X] \otimes |\Psi^+\rangle\langle\Psi^+|$ . Therefore, the probability of measuring  $s = 0$  is given by  $p(s = 0) = 1 - 2p_x + 2p_x^2$ . Hence, the probability of obtaining the legitimate quantum state  $\rho$  while measuring  $s = 0$  is given by  $p(\rho \cap s = 0) = 1 - 2p_x + p_x^2$ . The success probability  $p_s$  of arriving at the legitimate quantum state  $\rho$  given that the syndrome value is  $s = 0$  becomes  $p_s = p(\rho | s = 0) = \frac{1 - 2p_x + p_x^2}{1 - 2p_x + 2p_x^2}$ , which gives us a quadratic performance improvement over uncoded QBER as a function of  $p$ . The yield can be directly determined according to Def. 2 and the proof follows.

#### APPENDIX C: PROOF OF COROLLARY 2

The supermap of Eq. (9) based on the error-detection scheme proposed in Fig. 4 operating in the face of quantum phase-flip channels is given by  $\mathcal{S}(\bar{\rho}) = [(1 - p_z)^2 \rho + p_z(1 - p_z)Z \rho Z] \otimes |\Phi^+\rangle\langle\Phi^+| + [p_z^2 \rho + p_z(1 - p_z)Z \rho Z] \otimes |\Phi^-\rangle\langle\Phi^-|$ . Therefore, the probability of measuring

$s = 0$  is given by  $p(s = 0) = 1$ , since the measurement is carried out in the  $Z$  basis. Hence, the probability of measuring  $s = 0$  and obtaining the legitimate quantum state  $\rho$  is  $p(\rho \cap s = 0) = 1 - 2p_z + 2p_z^2$ . The yield can be directly determined according to Def. 2 and the proof follows.

#### APPENDIX D: PROOF OF PROPOSITION 2

After applying the first CNOT of the decoder  $\mathcal{V}_B^\dagger$  of Fig. 9, we can determine the probability of obtaining the syndrome value  $s_Z = 0$  from the first EPR pair as  $p(s_Z = 0) = 1 - \frac{4p}{3} + \frac{8p^2}{9}$ . If  $s_Z = 1$ , we discard the logical qubit. If  $s_Z = 0$ , the first-two quantum depolarizing channels are reduced into a single depolarizing channel having Kraus operators:  $N_1 = \sqrt{\frac{1-2p+\frac{10p^2}{9}}{1-\frac{4p}{3}+\frac{8p^2}{9}}}I$ ,  $N_2 = \sqrt{\frac{\frac{2p^2}{9}}{1-\frac{4p}{3}+\frac{8p^2}{9}}}X$ ,  $N_3 = \sqrt{\frac{\frac{2p^2}{9}}{1-\frac{4p}{3}+\frac{8p^2}{9}}}Y$ , and  $N_4 = \sqrt{\frac{\frac{2p}{3}-\frac{2p^2}{3}}{1-\frac{4p}{3}+\frac{8p^2}{9}}}Z$ . By applying the second CNOT of the decoder  $\mathcal{V}_B^\dagger$  of Fig. 9, we can determine the probability of obtaining the syndrome value  $s_X = 0$  from the second EPR pair as  $p(s_X = 0) = \frac{1-\frac{8p}{3}+\frac{26p^2}{9}-\frac{26p^3}{27}}{1-\frac{4p}{3}+\frac{8p^2}{9}}$ . The probability of arriving at the legitimate quantum state  $\rho$  and measuring the syndrome value  $s_X = 0$  is  $p(\rho \cap (s_X = 0)) = \frac{1-3p+\frac{28p^2}{9}-\frac{28p^3}{27}}{1-\frac{4p}{3}+\frac{8p^2}{9}}$ . By using Def. 1 and 2, the proof follows.

#### APPENDIX E: PROOF OF PROPOSITION 3

Similar to the proof of Prop. 1, By exploiting the error model of Section II-A and relying on the quantum encoder and decoder of Fig. 10, the supermap of Eq. (9) can be readily obtained. After the decoding operation, the first EPR pair is measured in the  $X$  basis while the second one in the  $Z$  basis. Let us distinguish the components of the syndrome string in Eq. (10) according to the basis used for the measurement. Specifically, let us denote the syndrome component obtained when the second EPR pair is measured in the  $Z$  basis by  $s_Z = s_A \oplus s_B$ , while the syndrome component obtained when the first EPR pair is measured in the  $X$  basis by  $s_X = s_A \oplus s_B$ . The overall syndrome string is  $\underline{s} = s_X s_Z$ . Since no error operators exhibiting even numbers of  $X$  errors and even numbers of  $Z$  errors can be detected, which gives us the syndrome vector of  $\underline{s} = 00$ , the probability we retain the logical qubits is equal to the sum of the probabilities of all these possible error patterns resulting in the syndrome vector of  $\underline{s} = 00$ . After observing  $4^4 = 256$  error patterns and by accounting for Eq. (9), we have  $p(\underline{s} = 00) = 1 - 4p + 8p^2 - \frac{64p^3}{9} + \frac{64p^4}{27}$ , which is obtained from one all-identity error pattern, 18 error patterns having a weight of two, 24 error patterns having a weight of three, and 21 error patterns having a weight of four, which generate the syndrome vector  $\bar{s} = 00$ . However, from all of those error patterns, only four of the error patterns that are actually associated with the legitimate quantum state  $\rho$  of the logical qubits, which are  $P \in \{IIII, XXXX, YYYY, ZZZZ\}$ . Hence, the probability of obtaining the legitimate

$$\begin{aligned}
\mathcal{S}(\bar{\rho}) = & (1-p_x)^4 \rho \otimes \rho_{\Phi+} \otimes \rho_{\Phi+} + p_x^2(1-p_x)^2 (IX)\rho(IX)^\dagger \otimes \rho_{\Phi+} \otimes \rho_{\Phi+} \\
& + p_x^2(1-p_x)^2 (XI)\rho(XI)^\dagger \otimes \rho_{\Phi+} \otimes \rho_{\Phi+} + p_x^2(1-p_x)^2 (XX)\rho(XX)^\dagger \otimes \rho_{\Phi+} \otimes \rho_{\Phi+} \\
& + p_x^4 \rho \otimes \rho_{\Psi+} \otimes \rho_{\Phi+} + p_x^2(1-p_x)^2 (IX)\rho(IX)^\dagger \otimes \rho_{\Psi+} \otimes \rho_{\Phi+} \\
& + p_x^2(1-p_x)^2 (XI)\rho(XI)^\dagger \otimes \rho_{\Psi+} \otimes \rho_{\Phi+} + p_x(1-p_x)^3 (XX)\rho(XX)^\dagger \otimes \rho_{\Psi+} \otimes \rho_{\Psi+} \\
& + p_x^2(1-p_x)^2 (XX)\rho(XX)^\dagger \otimes \rho_{\Psi+} \otimes \rho_{\Phi+} + p_x(1-p_x)^3 \rho \otimes \rho_{\Phi+} \otimes \rho_{\Psi+} \\
& + p_x(1-p_x)^3 (IX)\rho(IX)^\dagger \otimes \rho_{\Phi+} \otimes \rho_{\Psi+} + p_x(1-p_x)^3 (XI)\rho(XI)^\dagger \otimes \rho_{\Phi+} \otimes \rho_{\Psi+} \\
& + p_x^3(1-p_x) (XX)\rho(XX)^\dagger \otimes \rho_{\Phi+} \otimes \rho_{\Psi+} + p_x^3(1-p_x) \rho \otimes \rho_{\Psi+} \otimes \rho_{\Psi+} \\
& + p_x^3(1-p_x) (IX)\rho(IX)^\dagger \otimes \rho_{\Psi+} \otimes \rho_{\Psi+} + p_x^3(1-p_x) (XI)\rho(XI)^\dagger \otimes \rho_{\Psi+} \otimes \rho_{\Psi+}. \quad (41)
\end{aligned}$$

quantum state  $\rho$  while measuring  $\underline{s} = 00$  is  $p(\rho \cap (\underline{s} = 00)) = 1 - 4p + 6p^2 - 4p^3 + \frac{28p^4}{27}$ . By using Def. 1 and 2, the proof follows.

#### APPENDIX F: PROOF OF COROLLARY 3

Based on  $\mathcal{V}_A$  and  $\mathcal{V}_B^\dagger$  in Fig. 10 as well as on the Kraus operators of quantum bit-flip channel, we specify Eq. (9) as in Eq. (41) given at the top of this page, where  $\rho_{\Phi+} \triangleq |\Phi^+\rangle\langle\Phi^+|$  and  $\rho_{\Psi+} \triangleq |\Psi^+\rangle\langle\Psi^+|$ . In our scheme proposed in Fig. 10, we measure the first EPR pair in the  $X$  basis and the second EPR pair in the  $Z$  basis. For the sake of  $X$  error-detection, we decide to discard the logical qubits if we measure  $\rho_{\Psi+}$  for the second EPR pair, which can be inferred from classical measurement results  $s_Z = s_A \oplus s_B = 1$ . By contrast, we retain the logical qubits if we measure  $\rho_{\Phi+}$ , which implies  $s_Z = s_A \oplus s_B = 0$ . Therefore, from Eq. (41), the probability of getting the syndrome value of  $s_Z = 0$  from the second EPR pair is  $p(s_Z = 0) = 1 - 4p_x + 12p_x^2 - 16p_x^3 + 8p_x^4$ . It is important to observe that any error operator exhibiting odd numbers of  $X$  errors can be detected and the logical qubits are discarded. By contrast, any error operator exhibiting even numbers of  $X$  errors cannot be detected and hence the logical qubits are retained. There are two possible error patterns that preserve the legitimate encoded state of the logical qubits, i.e.  $P \in \{IIII, XXXX\}$ . Then, we have  $p(\rho \cap (s_2 = 0)) = 1 - 4p_x + 6p_x^2 - 4p_x^3 + 2p_x^4$ . By using Def. 1 and 2, the proof follows.

#### APPENDIX G: PROOF OF COROLLARY 4

Similar to App. F, but by using the Kraus operators of the quantum phase-flip channel, the supermap of Eq. (9) can be readily obtained. We discard the logical qubits if we measure  $|\Phi^-\rangle\langle\Phi^-|$  on the first EPR pair, i.e. when  $s_X = s_A \oplus s_B = 1$ . By contrast, we retain the logical qubits if we measure  $|\Phi^+\rangle\langle\Phi^+|$ , i.e. when  $s_X = s_A \oplus s_B = 0$ . Hence, we obtain  $p(s_X = 0)$  from the first EPR pair upon measurement is  $p(s_X = 0) = 1 - 4p_z + 12p_z^2 - 16p_z^3 + 8p_z^4$ . Similarly, any error operators exhibiting even numbers of  $Z$  errors cannot be detected and hence the logical qubits are retained. There are two possible error patterns that preserve the

legitimate encoded state of the logical qubits, i.e.  $P \in \{IIII, ZZZZ\}$ . Therefore, we obtain  $p(\rho \cap (s_X = 0)) = 1 - 4p_z + 6p_z^2 - 4p_z^3 + 2p_z^4$ . By using Def. 1 and 2, the proof follows.

## REFERENCES

- [1] H. J. Kimble, “The quantum Internet,” *Nature*, vol. 453, no. 7198, pp. 1023–1030, 2008.
- [2] M. Caleffi, A. S. Cacciapuoti, and G. Bianchi, “Quantum Internet: From communication to distributed computing!,” in *Proc. of the 5th ACM International Conference on Nanoscale Computing and Communication*, pp. 1–4, 2018.
- [3] S. Wehner, D. Elkouss, and R. Hanson, “Quantum Internet: A vision for the road ahead,” *Science*, vol. 362, no. 6412, 2018.
- [4] C. Wang, A. Rahman, and R. Li, “Applications and use cases for the quantum Internet,” Internet Draft draft-wang-qirg-quantum-internet-use-cases-04, Internet Engineering Task Force, Mar. 2020. Work in Progress.
- [5] M. Razavi, “Multiple-access quantum key distribution networks,” *IEEE Transactions on Communications*, vol. 60, no. 10, pp. 3071–3079, 2012.
- [6] D. Cuomo, M. Caleffi, and A. S. Cacciapuoti, “Towards a distributed quantum computing ecosystem,” *IET Quantum Communication (Invited Paper)*, vol. 1, no. 1, pp. 3–8, 2020.
- [7] M. Caleffi, D. Chandra, D. Cuomo, S. Hassanpour, and A. S. Cacciapuoti, “The rise of the quantum Internet,” *Computer*, vol. 53, no. 6, pp. 67–72, 2020.
- [8] Z. Sun, L. Song, Q. Huang, L. Yin, G. Long, J. Lu, and L. Hanzo, “Toward practical quantum secure direct communication: A quantum-memory-free protocol and code design,” *IEEE Transactions on Communications*, vol. 68, no. 9, pp. 5778–5792, 2020.
- [9] A. S. Cacciapuoti, M. Caleffi, F. Tafuri, F. S. Cataliotti, S. Gherardini, and G. Bianchi, “Quantum Internet: Networking challenges in distributed quantum computing,” *IEEE Network*, vol. 34, no. 1, pp. 137–143, 2019.
- [10] A. S. Cacciapuoti, M. Caleffi, R. Van Meter, and L. Hanzo, “When entanglement meets classical communications: Quantum teleportation for the quantum Internet,” *IEEE Transactions on Communications (Invited Paper)*, vol. 68, no. 6, pp. 3808–3833, 2020.
- [11] M. A. Nielsen and I. L. Chuang, *Quantum computation and quantum information*. Cambridge University Press, 2000.
- [12] G. Cariolaro and G. Pierobon, “Performance of quantum data transmission systems in the presence of thermal noise,” *IEEE Transactions on Communications*, vol. 58, no. 2, pp. 623–630, 2010.
- [13] C. E. Shannon, “A mathematical theory of communication,” *The Bell System Technical Journal*, vol. 27, no. 3, pp. 379–423, 1948.
- [14] P. W. Shor, “Scheme for reducing decoherence in quantum computer memory,” *Phys. Rev. A*, vol. 52, no. 4, 1995.
- [15] A. R. Calderbank and P. W. Shor, “Good quantum error-correcting codes exist,” *Phys. Rev. A*, vol. 54, no. 2, 1996.
- [16] R. Laflamme, C. Miquel, J. P. Paz, and W. H. Zurek, “Perfect quantum error correcting code,” *Phys. Rev. Lett.*, vol. 77, no. 1, 1996.
- [17] D. A. Lidar and T. A. Brun, *Quantum error correction*. Cambridge University Press, 2013.
- [18] Z. Babar, D. Chandra, H. V. Nguyen, P. Botsinis, D. Alanis, S. X. Ng, and L. Hanzo, “Duality of quantum and classical error correction codes: Design principles and examples,” *IEEE Communications Surveys & Tutorials*, vol. 21, no. 1, pp. 970–1010, 2018.
- [19] Y. Fujiwara, D. Clark, P. Vandendriessche, M. De Boeck, and V. D. Tonchev, “Entanglement-assisted quantum low-density parity-check codes,” *Phys. Rev. A*, vol. 82, no. 4, 2010.
- [20] M. M. Wilde and J. M. Renes, “Quantum polar codes for arbitrary channels,” in *Proc. of the IEEE International Symposium on Information Theory (ISIT)*, pp. 334–338, IEEE, 2012.
- [21] M. M. Wilde, M.-H. Hsieh, and Z. Babar, “Entanglement-assisted quantum turbo codes,” *IEEE Transactions on Information Theory*, vol. 60, no. 2, pp. 1203–1222, 2013.

- [22] D. Chandra, Z. Babar, H. V. Nguyen, D. Alanis, P. Botsinis, S. X. Ng, and L. Hanzo, “Quantum coding bounds and a closed-form approximation of the minimum distance versus quantum coding rate,” *IEEE Access*, vol. 5, pp. 11557–11581, 2017.
- [23] T. A. Brun, I. Devetak, and M.-H. Hsieh, “Correcting quantum errors with entanglement,” *Science*, vol. 314, no. 5798, pp. 436–439, 2006.
- [24] I. Devetak, T. A. Brun, and M.-H. Hsieh, “Entanglement-assisted quantum error-correcting codes,” in *New Trends in Mathematical Physics: Selected Contributions of the 15th International Congress on Mathematical Physics*, pp. 161–172, Springer, 2009.
- [25] M. Grassl, “Entanglement-assisted quantum communication beating the quantum Singleton bound,” in *Proc. of the 16th Asian Quantum Information Science Conference (AQIS)*, pp. 20–21, 2016.
- [26] C. H. Bennett, H. J. Bernstein, S. Popescu, and B. Schumacher, “Concentrating partial entanglement by local operations,” *Phys. Rev. A*, vol. 53, no. 4, 1996.
- [27] C. H. Bennett, G. Brassard, S. Popescu, B. Schumacher, J. A. Smolin, and W. K. Wootters, “Purification of noisy entanglement and faithful teleportation via noisy channels,” *Phys. Rev. Lett.*, vol. 76, no. 5, p. 722, 1996.
- [28] C. H. Bennett, D. P. DiVincenzo, J. A. Smolin, and W. K. Wootters, “Mixed-state entanglement and quantum error correction,” *Phys. Rev. A*, vol. 54, no. 5, 1996.
- [29] R. Matsumoto, “Conversion of a general quantum stabilizer code to an entanglement distillation protocol,” *Journal of Physics A: Mathematical and General*, vol. 36, no. 29, 2003.
- [30] C. H. Bennett, G. Brassard, C. Crépeau, R. Jozsa, A. Peres, and W. K. Wootters, “Teleporting an unknown quantum state via dual classical and Einstein-Podolsky-Rosen channels,” *Phys. Rev. Lett.*, vol. 70, no. 13, 1993.
- [31] M. Caleffi and A. S. Cacciapuoti, “Quantum switch for the quantum Internet: Noiseless communications through noisy channels,” *IEEE Journal on Selected Areas in Communications*, vol. 38, no. 3, pp. 575–588, 2020.
- [32] D. Chandra, Z. Babar, S. X. Ng, and L. Hanzo, “Near-hashing-bound multiple-rate quantum turbo short-block codes,” *IEEE Access*, vol. 7, pp. 52712–52730, 2019.
- [33] D. Chandra, Z. Babar, H. V. Nguyen, D. Alanis, P. Botsinis, S. X. Ng, and L. Hanzo, “Quantum topological error correction codes are capable of improving the performance of Clifford gates,” *IEEE Access*, vol. 7, pp. 121501–121529, 2019.
- [34] R. Cane, D. Chandra, S. X. Ng, and L. Hanzo, “Mitigation of decoherence-induced quantum-bit errors and quantum-gate errors using Steane’s code,” *IEEE Access*, vol. 8, pp. 83693–83709, 2020.
- [35] A. Steane, “Multiple-particle interference and quantum error correction,” *Proc. of the Royal Society of London. Series A: Mathematical, Physical and Engineering Sciences*, vol. 452, no. 1954, pp. 2551–2577, 1996.
- [36] J. Preskill, “Reliable quantum computers,” *Proc. of the Royal Society of London. Series A: Mathematical, Physical and Engineering Sciences*, vol. 454, no. 1969, pp. 385–410, 1998.
- [37] E. T. Campbell, B. M. Terhal, and C. Vuillot, “Roads towards fault-tolerant universal quantum computation,” *Nature*, vol. 549, no. 7671, pp. 172–179, 2017.
- [38] S. Bravyi and A. Kitaev, “Universal quantum computation with ideal Clifford gates and noisy ancillas,” *Phys. Rev. A*, vol. 71, no. 2, 2005.